ISSN 1349-1113
JAXA-RR-07-051E

JAXA Research and Development Report

A Parametric Study on Parallel Blade-Vortex Interaction for Helicopter Rotor

Yasutada TANABE, Shigeru SAITO, Keisuke TAKASAKI and Hajime FUJITA

February 2008

Japan Aerospace Exploration Agency

A Parametric Study on Parallel Blade-Vortex Interaction for Helicopter Rotor*

Yasutada Tanabe**, Shigeru Saito**, Keisuke Takasaki***, Hajime Fujita***

Abstract

A parametric study on parallel blade-vortex interaction (BVI) is carried out. A high accuracy CFD scheme and a fine grid system are employed to capture the vortex. By locating the initial vortex well upstream of the airfoil, a parallel vortex interaction is simulated. The results are compared with the existing experimental data with good agreement. The initial miss distance, airfoil incidence, vortex rotation directions are chosen as the parameters for this parametric study. The BVI strength shows a high dependency on the initial miss distance and the feature changes with the airfoil incidence. The maximum BVI level occurs at the initial miss distance lower than the leading edge of the airfoil when the airfoil has incidences. The cause of the maximum BVI location change is observed due to the upwash exists ahead of the incident airfoil, which moves the vortex upward while the vortex is convected by the flow. At the maximum BVI level, the final miss distance between the vortex and the airfoil is nearly zero, the head-on BVI as so-called.

Keywords: Parallel Blade-Vortex Interaction, Miss Distance, Incidence, Noise, Helicopter Rotor, Parametric Study

概　要

並行ブレード／渦干渉(BVI)についてパラメトリック研究を行った。渦を捕捉するために、高い精度の CFD スキームと細かい格子系を使用した。翼型の位置からかなり上流に初期渦を置き、下流に向けて一様流によって伝搬させることにより、渦糸が並行にブレードと干渉する流れ場をシミュレートした。迎え角がゼロの場合の結果については、既存の実験結果とも比較し、良い一致が見られた。初期ミス・ディスタンス、翼型の迎え角、渦の回転方向の三つがパラメータとして選ばれた。BVI の強さは初期ミス・ディスタンスによって大きく変化し、迎え角が変わると、その変化の特徴が違ってくる。翼型が迎え角をとると、 BVI レベルの最大値は翼型の前縁の垂直位置よりも低い初期ミス・ディスタンスのところで発生することが分かった。その原因としては、迎え角がある場合は、翼の前方に上向きの速度(アップワッシュ)が存在するため、渦が下流へ運ばれるときに上方向にも移動していることが観測された。実際の BVI の最大値は最終的には渦が直接翼とぶつかる、いわれるヘッドオン状態で発生しているが確認された。

Nomenclature

c	blade chord length
Cp	pressure coefficient
M_{tip}	hover tip Mach number
p	pressure
r	blade spanwise coordinate
R	rotor radius
SP	sound pressure
Z_v	initial vortex location relative to airfoil
α	angle of attack
Γ_v	vortex circulation
μ	rotor advance ratio
X_{bvi}	BVI pressure increment
L_{bvi}	BVI sound pressure increment
$M_{\infty i}$	free stream Mach number
V_∞	free stream velocity
ρ	density

1. Introduction

The Blade-Vortex-Interaction (BVI) is the main cause of the annoying noise and vibration for helicopter especially during the descending flight. The strongest part of this BVI phenomenon occurs while the blade strikes or passes closely the tip vortices shed from preceding blades nearly in parallel. So the understanding of parallel BVI is important to understand the major part of the BVI phenomena for a helicopter rotor. If we see from the blade and let the flow come from left hand side, in the advancing side of a rotor, the blade has less attack angle while the vortex rotating in counter-clockwise direction. On the other hand, in the retreating side of the rotor, the blade has larger attack angle and the vortex is rotating in clockwise direction.

There are several experiments and simulations on the parallel BVI till now. The representative parallel BVI experiment was carried out by Kitaplioglu et al. [1, 2], and it became a good test case for comparison with CFD simulations. In their experiment, a rotor blade with zero incidence strikes with a straight line vortex generated by an independent vortex generator located in the upstream. No researches on the BVI with incident airfoil are reported at this point. Numerical simulation of the parallel BVI was carried out by several researchers [3-7] with certain success to capture the main features. In previous researches, the numerical dissipation of the numerical schemes usually caused difficulties to preserve the initial vortex strength and structure during the free convection of the vortex during BVI process. The initial vortex was often located relatively in a short distance from the leading edge of the airfoil, leaving no enough time to remove

* Presented, in part, at the American Helicopter Society Specialists' Conference, International Forum on Rotorcraft Multidisciplinary Technology, Seoul, Korea, October 15-17, 2007.

** Safety and Operation Technology Team, Aviation Program Group (航空プログラムグループ、運航・安全技術チーム)

*** Nihon University (日本大学理工学部)

the initial computational disturbances caused by the sudden imposition of the vortex onto the initial steady flow. For a better understanding of this basic phenomenon and obtaining a quantitative relationship with BVI strength, initial miss distance and other factors, a parametric study has been carried out by the authors. Blade attack angle and blade nose to vortex center distance (the miss distance) are chosen as the parameters with the vortex rotating at two opposite directions.

For the simulation of parallel BVI, a vortex is initially put at a far upstream location and then passes through the blade airfoil vicinity. Overlapped grid approach [8] is utilized for the numerical simulation. In this approach, a Cartesian background grid is used to cover a wide range of computation area (called outer background grid) and another Cartesian background grid is located around the rotor to preserve the tip vortices wake (called inner background grid). The airfoil vicinity is surrounded by a body fitted curvilinear grid (called inner moving grid or airfoil grid for short). As the numerical dissipation of the vortex has been a key problem relating with the BVI simulation, a CFD scheme with high spatial accuracy is applied to the inner and outer background grids. Combined with a moderate fine inner background grid mesh size, the initial vortex is well preserved along a long distance of convection that ensures the overall accuracy of the simulation [3].

2. Test case

A basic test case is selected based on the experiment by Kitaplioglu et al. [1,2]. As shown in Fig. 1, a vortex generator is located in the upstream of a zero incidence rotor, and the blade interacts with the generated tip vortex when the blade is aligned with the wind tunnel flow stream line. Because the relative speed at each rotor radius position with regard to the vortex is different, only a narrow blade azimuth angle range and a limited blade section area can be regarded as a good condition to the ideal two-dimensional parallel BVI simulation.

For the present two-dimensional parallel BVI simulation as shown in Fig. 2, the flow condition is determined so that experimental data exists for the zero incidence case. The rotor blade section at $r/R = 0.876$ is instrumented with pressure sensors and is then selected for this study. Because the rotor tip Mach number is 0.714, a relative speed of Mach number 0.626 is used to meet the experimental condition.

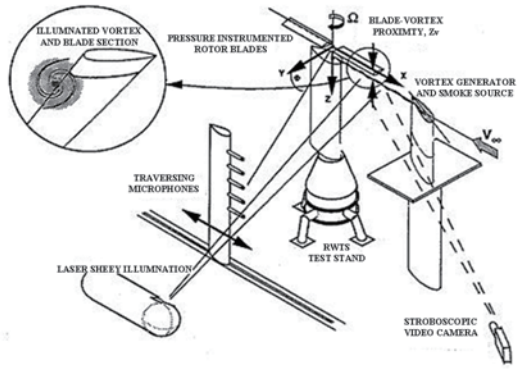

Fig. 1 Experimental Set-up [1,2]

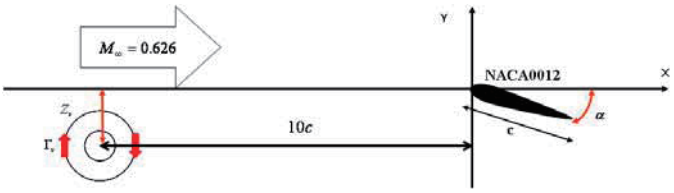

Fig. 2 Initial Condition

In the computations, distances are non-dimensionalized with respect to the blade chord length c, and the velocities are non-dimensionalized with respect to the free stream velocity. An initial vortex based on Scully vortex model [9] is used with circulation of 0.2536 and core radius of 0.162 to agree with the measurement [3].

The computational parameter cases are shown in Table 1. The computational accuracy is validated through the comparisons with experiments for the cases of zero incidence. Then the incidence angle is varied with the sweep of initial miss distance for both vortex rotation directions.

The miss distance of a vortex with an airfoil in the BVI study is usually referred to the vertical distance of the vortex to the airfoil leading edge when the vortex strikes on or aligns with the airfoil leading edge. But the vertical position of the vortex may change during the convection toward a lifting airfoil and is a result of the BVI process itself. So in this study, the initial miss distance is selected as the parameter and it may not necessarily agree with the miss distance when the vortex is aligned with the airfoil leading edge.

Table 1. Computational Parameter Cases

Initial miss distance Z_v [m]	0, -0.13, -0.25, -0.4, -1.0, -1.5
	0.13, 0.25, 0.4, 1.0, 1.5
Airfoil incidence α [deg]	0, 2, 4, 8
Vortex rotation	Clockwise, Counter-clockwise

3. Numerical method

3.1 Overlapped grid approach

The overlapped grid approach [8] is used for this study. As shown in Fig. 3, there are three layers of computational grid. A wide outer background grid with coarse grid resolution is used for preservation of the flow field boundary conditions. A fine resolution inner background grid is used to cover the path of vortex convection and preserve the initial vortex from numerical dissipation. An airfoil grid is used for the computation around the airfoil. For computational efficiency, Cartesian type grids are used for the background grids and a 4th order high resolution numerical scheme based on SHUS scheme [10] is used. For time integration, 4 stage Runge-Kutta method suggested by Jameson et al. [11] is used. The airfoil grid is curvilinear, and a 2nd order Yee-Harten TVD scheme [12] is adopted.

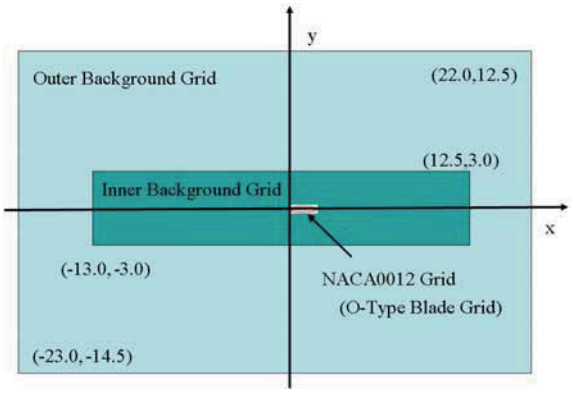

(a) Whole computational Domain

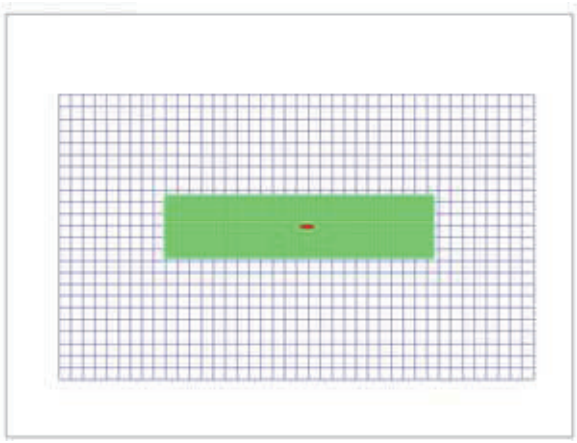

(b) Overlapped Grids Used

Fig. 3 Moving Overlapped Grid Approach

3.2 CFD procedure

Figure 4 shows CFD procedure for overlapped grid approach. The computation starts from the outer background, and then computation in inner background grid is executed with the boundary values interpolated from the outer background grid. Then, with the outer boundary values obtained from the inner background grid, computation in the airfoil grid is advanced. The whole airfoil grid values are interpolated onto the overlapped area with the inner background grid. Finally, inner background grid values are interpolated onto the overlap area with the outer background grid to finish one cycle of computation.

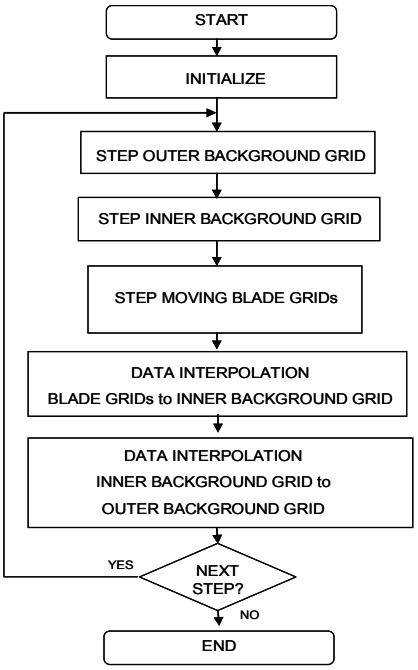

Fig. 4 CFD procedure for Overlapped Grid Approach

For present study, a common time step is pre-designated and the information is exchanged between each layer of grid at this time step. And for computation in each layer of grid, divided time steps are used to meet the each given maximum allowable CFL number. Because the numerical scheme for the background grid is an explicit one, a CFL number is given less than 0.8. For the inner airfoil grid, a CFL number is given less than 25. With such strategy, an efficient and robust simulation code is developed.

The governing equations applied in the background grids are Euler equations. Although the CFD solver applied in the airfoil grid is an Euler/Navier-Stokes equation solver, only the inviscid Euler option was used in this study. Viscous effect on the parallel BVI is considered not dominant and will be studied later.

4. Results and Discussion

4.1 Dissipation of vortex during convection

For the simulation of BVI, the preservation of the vortex is the key to the accurate solution. In the previous study, three different inner background grid sizes were tested [3]. As shown in Fig. 5, a grid size of 0.0125c at least is required to keep the vortex non-dissipated during the long convection process. This grid size is used for the following BVI simulations.

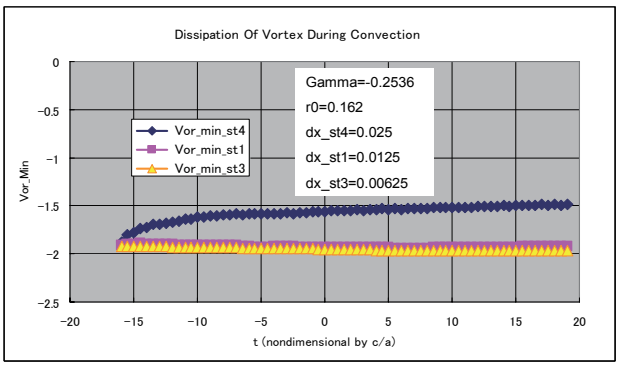

Fig. 5 Dissipation of vortex during convection for different grid resolutions [3]

4.2 Flow field changes during BVI

For the visualization of the pressure change (so as the sonic wave) in the flowfield, the difference of pressure for a certain time step (a numerical approximation to pressure time gradient, namely, the sonic wave) is plotted in Figs. 6 and 7. The sonic wave emitted from the airfoil after the vortex passed is significantly emphasized. One case (Fig. 6) is that the incidence angle is zero degree and the miss distance is also zero (so-called head-on case). The other case (Fig. 7) is that the incidence angle is four degrees and the initial miss distance is zero. It can be seen that the sonic wave is weaker in the incidence 4 degrees case. In these plots, the positions of the sound pressure pickup sensor are indicated and will be explained in detail in Fig. 15.

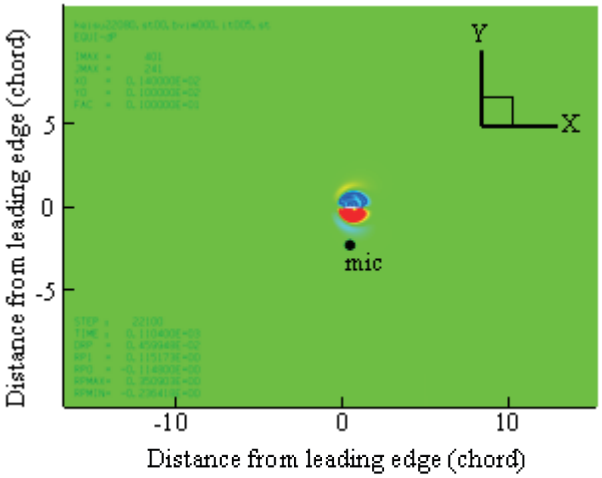

(a) 0.5 (non-dimensional time)

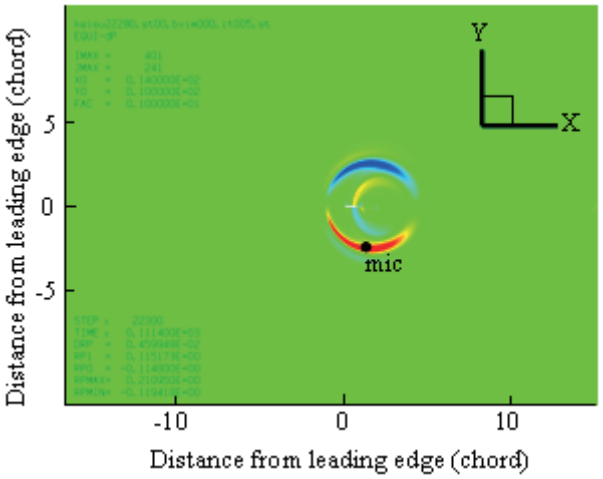

(b) 1.5 (non-dimensional time)

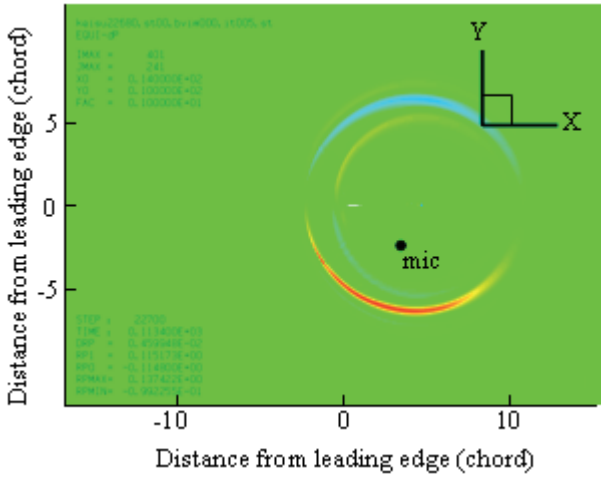

(c) 3.5 (non-dimensional time)

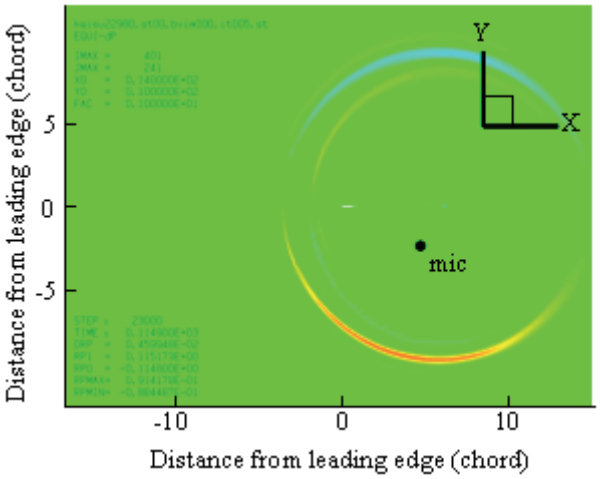

(d) 5.0 (non-dimensional time)

Fig. 6 $\Delta p/\Delta t$ contours for $\alpha = 0°$, $\Gamma_v = -0.252$

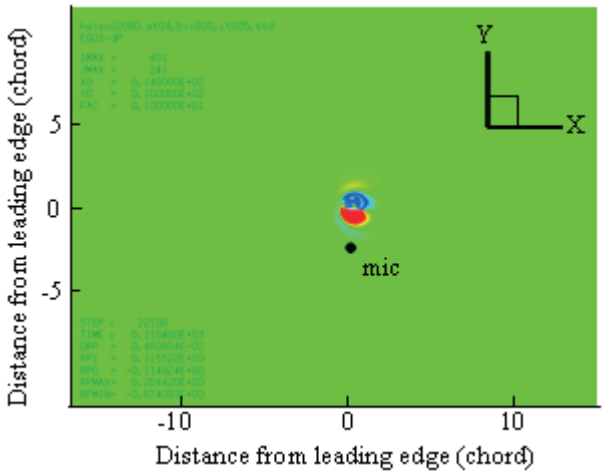

(a) 0.5 (non-dimensional time)

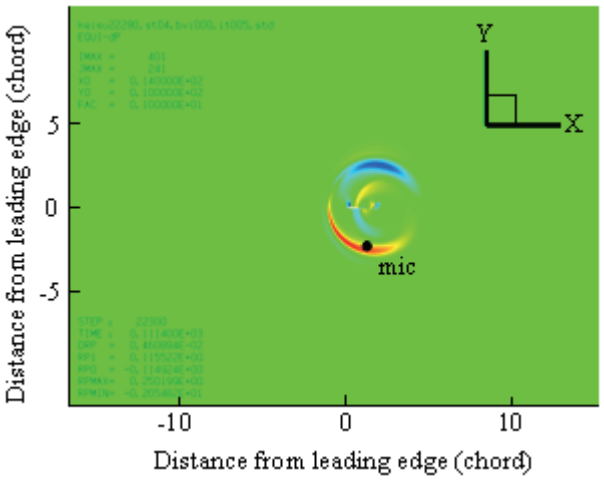

(b) 1.5 (non-dimensional time)

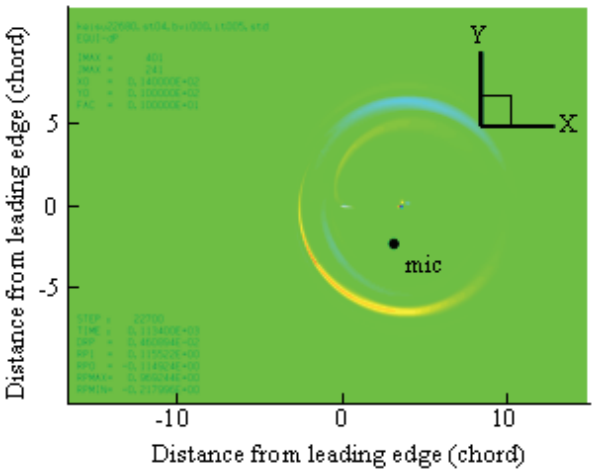

(c) 3.5 (non-dimensional time)

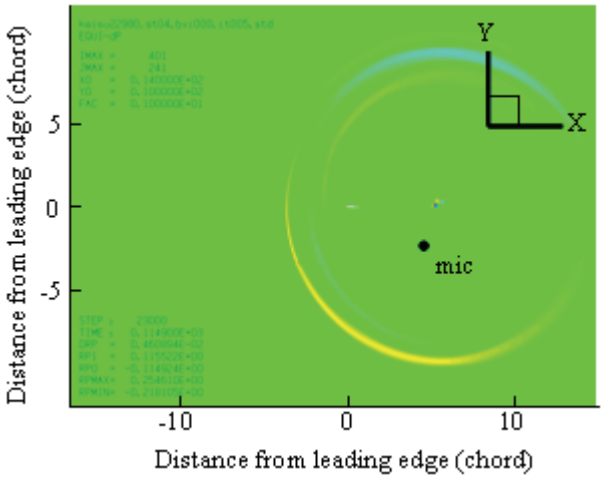

(d) 5.0 (non-dimensional time)

Fig. 7 $\Delta p/\Delta t$ contours for $\alpha = 4°$, $\Gamma_v = -0.252$

4.3 Comparison of pressure changes with experiment

Comparison of the surface pressure with the existing experiment result shows good agreement in Fig. 8. When the vortex reaches the blade leading edge, the lower surface pressure begins an abrupt increase. The effect of this fast BVI wave (red line area) appears to be the establishment of a fairly steady pressure level that persists for some duration. And the effect of the second BVI wave (blue line area) appears when the vortex passes away from the airfoil. These second BVI waves go from trailing edge to leading edge. These phenomena can be seen in both computation and experiment with good agreements. It is concluded that the CFD method can be used to correctly predict the influence of the variation of BVI strength on the change of miss distance and other parameters.

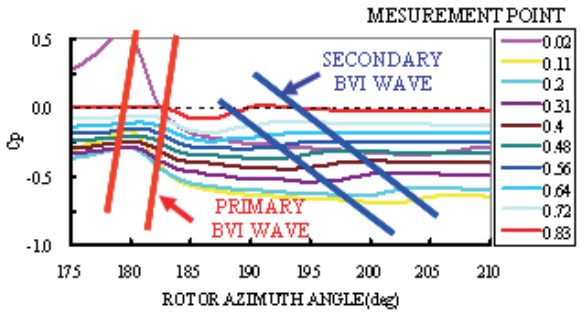

(a) Computation

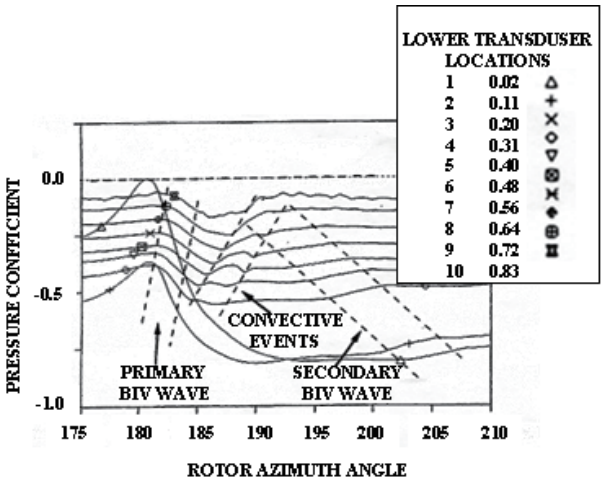

(b) Experiment[1, 2]

Fig. 8 Blade pressure variations induced by parallel BVI, results comparisons with computation and experiment.

4.4 BVI level evaluations

To evaluate the BVI level, a factor X_{bvi} is introduced by Kitaplioglu et al [1, 2] as in Fig. 9. It is a measurement of the pressure fluctuaion caused by BVI. Subscript _up is for the pressure fluctuation on the upper surface while _lo is for the lower surface on the blade. Summation of these two values is defined as X_{bvi_sum} and is used as a measurement of the BVI level.

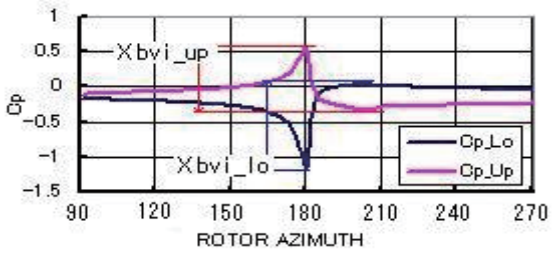

Fig. 9 Calculation of X_{bvi}

The problem of this method is we must know which position is most suitable to sense the BVI. Figure 10 shows the comparison of the BVI level X_{bvi_sum} at leading edge area 0~6%c for attack angles $\alpha = 0° \sim 8°$. From this figure, we can see that the pressure changes at position from 1%c~3%c on the leading edge is most suitable for the BVI phenomenon identification. As a steady and high point, we have selected 2%c as the representative location to pick up the pressure for BVI level evaluations. It is noticeable that the leading edge point 0c is less insensitive to the BVI phenomenon. Also remember the airfoil under study is a symmetrical profile and this position may shift when airfoil profile changes.

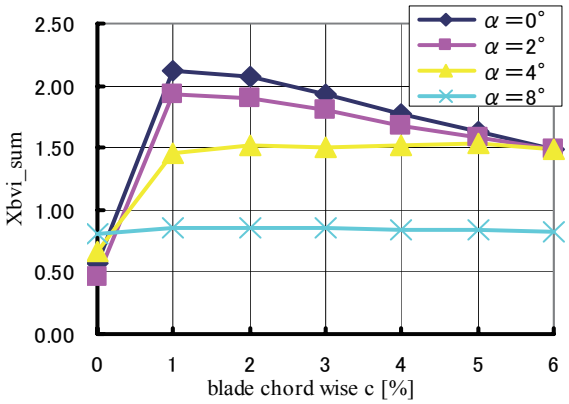

Fig. 10 BVI pressure at leading edge for $\alpha = 0° \sim 8°$

Figure 11 shows the summation of the upper and lower X_{bvi} with regard to the miss distance for incidence of 0 degree. It can be seen that the BVI level drops to nearly one half when the initial miss distance is 0.5c. The maximum BVI level occurs at zero miss distance (the head-on case).

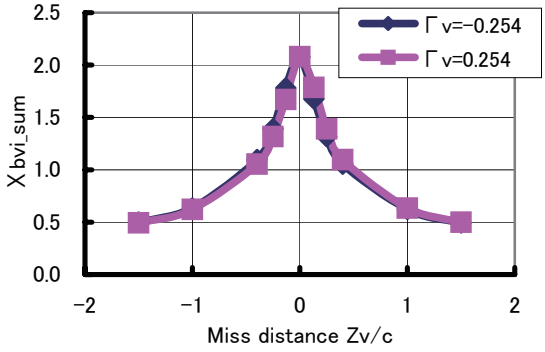

Fig. 11 X_{bv_sum} vs. initial miss distance for $\alpha = 0°$

Figure 12 shows the comparison of BVI level with experiment. The computational result of the positive vortex agrees with the experimental result quite well. The computational results for the negative rotational vortex are symmetric to the zero initial miss distance and are considered reasonable.

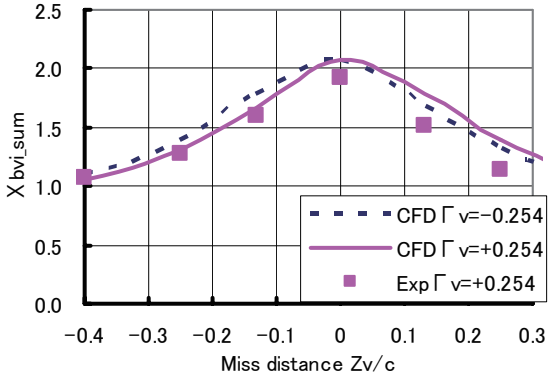

Fig. 12 Comparison of X_{bvi_sum} vs. miss distance for $\alpha = 0°$ with experiment

Figure 13 is the BVI level X_{bv_sumi} for incidence angle of 4 degrees. The maximum BVI level occurs at a negative initial miss distance instead of the zero initial miss distance.

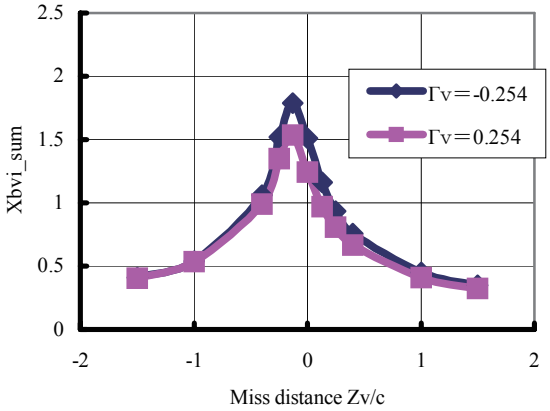

Fig. 13 X_{bvi_sum} vs. initial miss distance for $\alpha = 4°$

As another BVI level evaluation factor, L_{bvi} is determined for the sound pressure change as shown in Figure 14 following the definition by Kitaplioglu et al [1, 2]. It is defined as a direct measurement of the noise level caused by BVI. The selected microphone in the near-field of the interaction is microphone #7 as defined in ref [1] (also shown in Fig. 15). And the microphone traverses with vortex to obtain the sound signal equivalent to experiment. The microphone positions are indicated in plots in Fig. 7. The time scale in Fig. 14 is shifted so that the nondimensional time DT is 0 when the vortex is just convected by flow to the airfoil leading edge position.

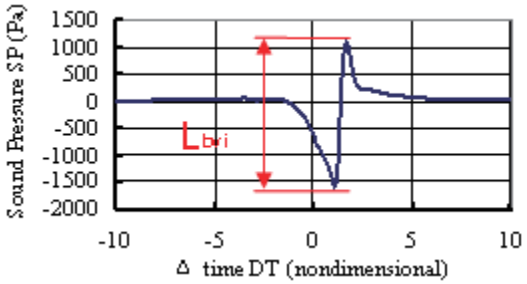

Fig. 14 Calculation of L_{bvi} ($\Gamma_v = -0.252$, $\alpha = 0°$, $Z_v/c = 0$, mic7)

Evaluation factor L_{bvi} obtained from microphone #7 is a direct measurement of the near-field BVI noise because it is the pressure jump in the flowfield associated with the BVI event. As shown in Figs. 16, 17 and 18, there seems have good correlation with the X_{bvi} which is based on the surface pressure change. And the miss distance for the maximum L_{bvi} at 2 and 4 degrees also moves to negative side.

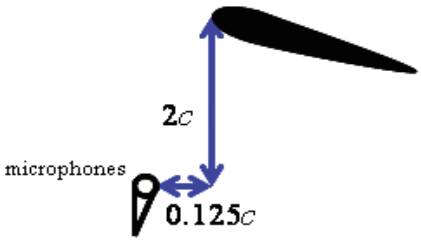

Fig. 15 Near-field microphone positions

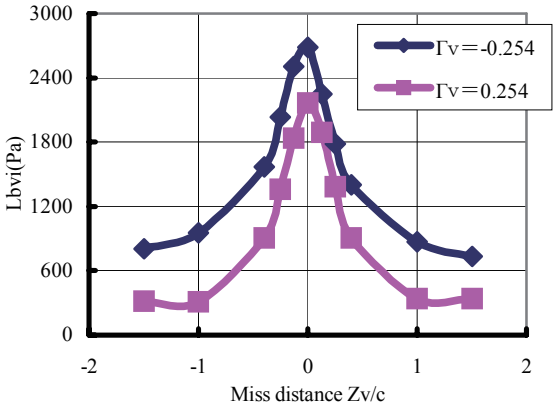

Fig. 16 L_{bvi} vs. miss distance for $\alpha = 0°$

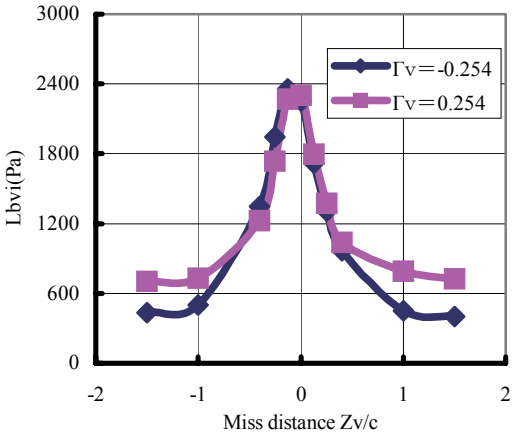

Fig. 17 L_{bvi} vs. miss distance for $\alpha = 2°$

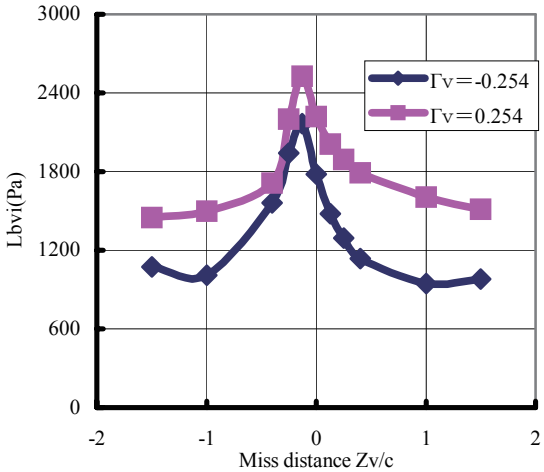

Fig. 18 L_{bvi} vs. initial miss distance for $\alpha = 4°$

The peak values of X_{bvi_sum} and L_{bvi} with regard to the incidence angle is shown in Fig. 19. It can be seen that the peak values of X_{bvi_sum} decrease with incidence angle both for positive and negative vortex. But for L_{bvi}, the relation is opposite for opposite direction vortices. The reason of this

reversion can be explained by using Fig. 6 at first. When the vortex is negative (clockwise rotation), the BVI sonic wave in the upper plane of the airfoil firstly have a positive pressure rise front followed by a deep decrease, and in the lower plane where the sonic pickup microphone placed, the BVI sonic wave decrease lightly at first followed by a abrupt increase. The pressure signals sensed by the microphone for different initial miss distances are shown in Fig. 20. For a positive vortex, the pressure signal at same microphone position is shown in Fig. 21. Although the flowfields are symmetric with regard to the different vortex direction, because the microphone is fixed at the lower plane, the sonic signals are not symmetric and there were level differences for same initial miss distances. When there is incidence angle of the airfoil, the original pressure distribution at the lower plane of the airfoil has a slow rise near the airfoil which is the source of the well-known loading noise. Combined with the BVI related pressure change, the pressure jump levels are alleviated. The pressure signals for incidence angle 4 degrees for positive and negative vortex is shown in Fig. 22 and 23.

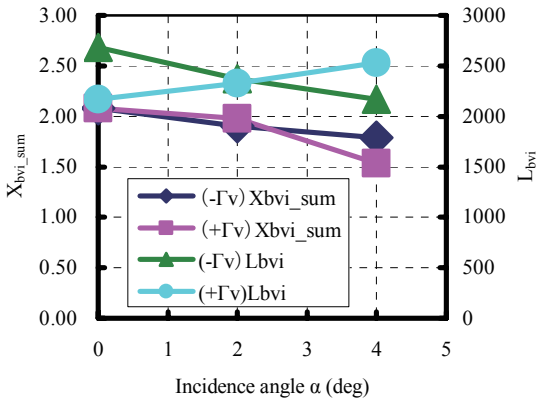

Fig. 19 Peak values of X_{bvi_sum} and L_{bvi} vs airfoil incidence angle

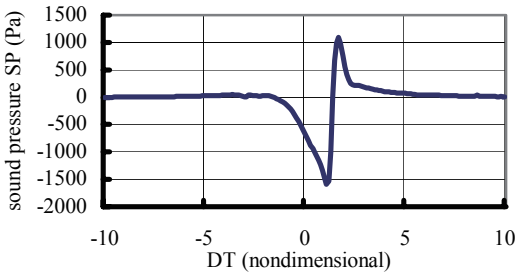

(a) $Z_v/c=0$

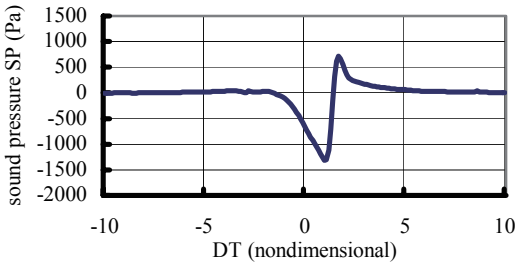

(b) $Z_v/c=-0.25$

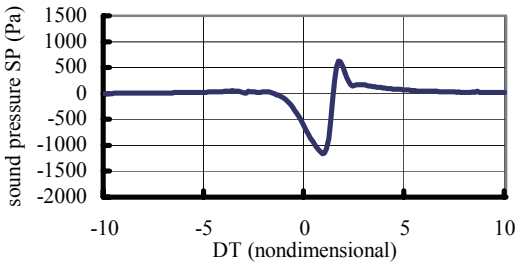

(c) $Z_v/c=0.25$

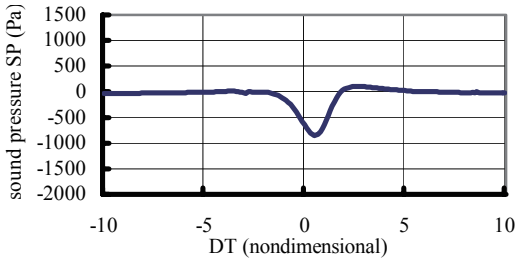

(d) $Z_v/c=-1.00$

Fig.20 Near-field microphone 7 for $\alpha=0°$, $\Gamma_v=-0.252$

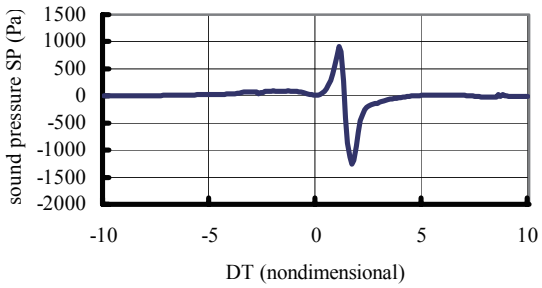

(a) $Z_v/c=0$

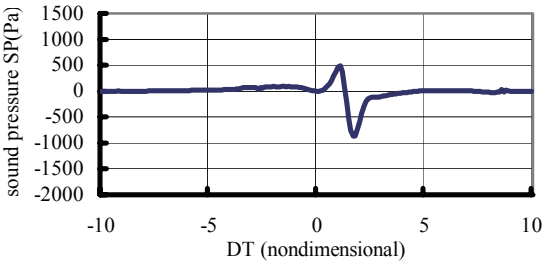

(b) $Z_v/c=-0.25$

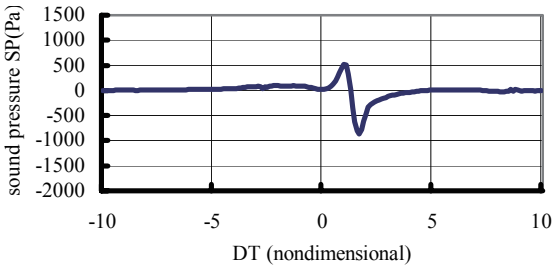

(c) $Z_v/c=0.25$

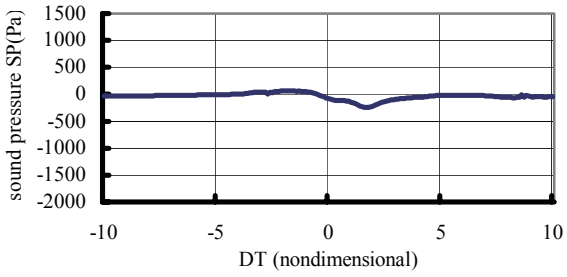

(d) $Z_v/c=-1.00$

Fig.21 Near-field microphone 7 for $\alpha=0°$, $\Gamma_v=0.252$

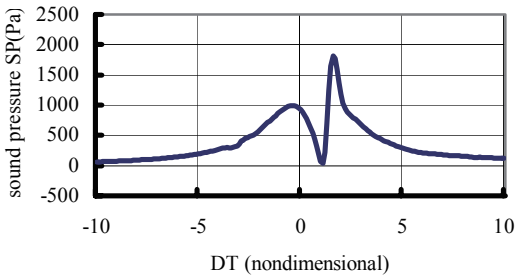

(a) $Z_v/c=0$

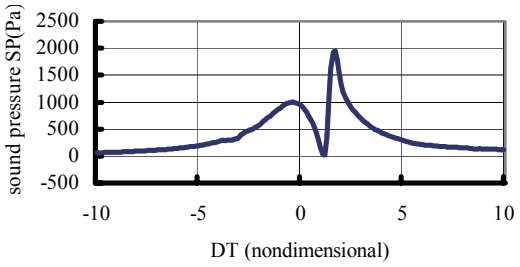

(b) $Z_v/c=-0.25$

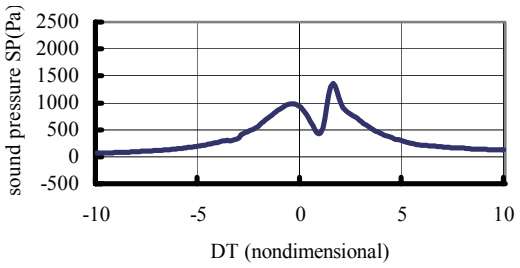

(c) $Z_v/c=0.25$

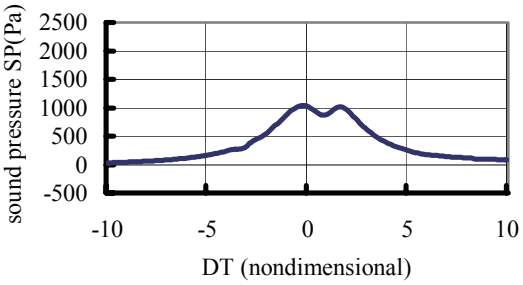

(d) $Z_v/c=-1.00$

Fig.22 Near-field microphone 7 for $\alpha=4°, \Gamma_v=-0.252$

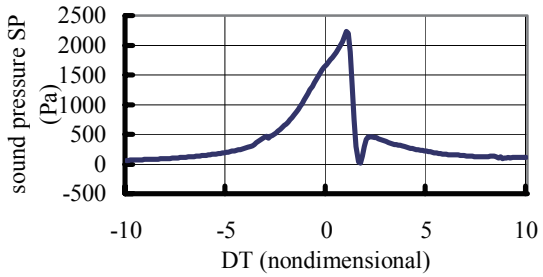

(a) $Z_v/c=0$

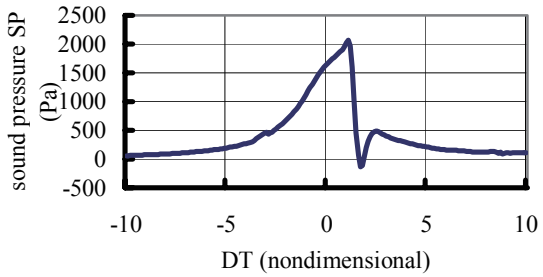

(b) $Z_v/c=-0.25$

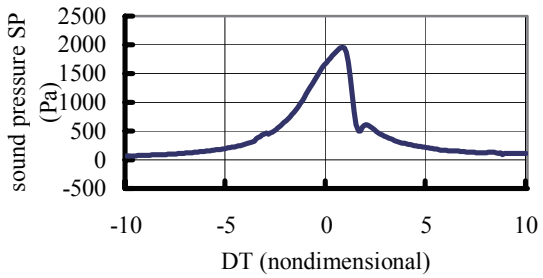

(c) $Z_v/c=0.25$

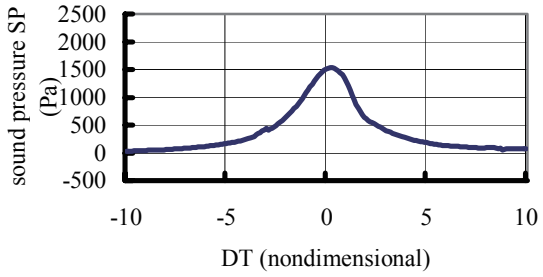

(d) $Z_v/c=-1.00$

Fig.23 Near-field microphone 7 for $\alpha=4°$, $\Gamma_v=0.252$

4.5 BVI peak level position change with incident angle

As the incidence angle of the airfoil is increased, the initial miss distance of the maximum of the BVI level shift to negative side in all cases. The BVI peak locations for incident angle from 2 to 8 degrees are shown in Fig. 24. There were no differences observed in the peak level position between positive and negative vortices. Although there are some discrepancies especially for 2 degrees points, it can be seen the peak position shifts are nearly linearly decrease with the incidence angle of the airfoil.

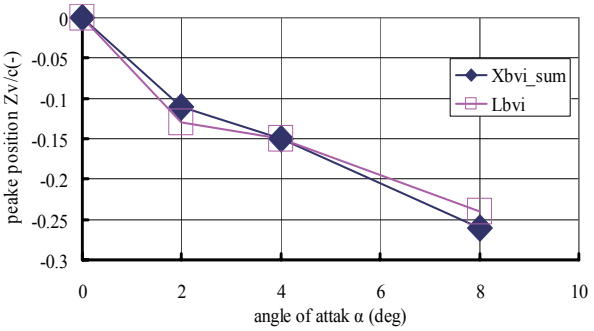

Fig. 24 BVI level peak position vs incidence angle

The reason to cause such shifts is investigated by plotting the trajectories of the vortex while it is convected by the flow downstream. Firstly, to check if there is vertical movement of a vortex when the incidence angle is zero, the vortex trajectory is plotted in Fig. 25. It can be seen there is no noticeable vertical position change of the vortex in this case. It is concluded that there is no noticeable miss distance shift caused by the vortex itself. In Fig. 26, the airfoil incidence is 8 degrees. Fig.26(a) is for a vortex initially located at Zv/c=0. As it is convected downstream, the vortex moves upward and its core center misses the airfoil leading edge. In Fig.26(b), the vortex initially located Zv/c=-0.25. When it is convected by the flow, the core center of this vortex strikes the leading edge directly as a head-on interaction and causes maximum level of BVI. The upward movement of vortex is caused by the upwash flow ahead of an airfoil with incidence angle. Also the strength of upwash is nearly proportional to the incident angle. So the relation shown in Fig.24 can be reasonably explained.

Fig. 25 Vortex trajectory for $\alpha=0^\circ$, Zv/c=0.00, clockwise vortex

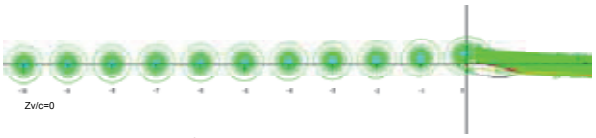

(a) $\alpha = 8^\circ$, Zv/c=0.00, clockwise vortex

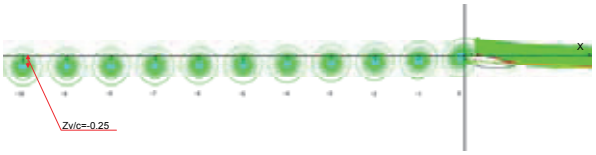

(b) $\alpha = 8^\circ$, Zv/c=-0.25, clockwise vortex

Fig. 26 Trajectories of vortex for $\alpha = 8^\circ$

5. Conclusions

In this study, the following conclusions are drawn.

1. A high accuracy CFD scheme and a fine grid system are employed to capture the vortex. Along with the convection of vortex, few dissipation of the initial vortex is observed which ensures the accuracy of current BVI simulations.

2. By locating the initial vortex well upstream of the airfoil, a parallel blade vortex interaction is simulated. Pressure changes at position from 1~3%*c* on the leading edge is most suitable for the BVI noise identification. The result of surface pressure and sound pressure changes are compared with the existing experimental data with good agreements.

3. The initial miss distance, airfoil incidence, vortex rotation directions are chosen as the parameters for this parametric study. The BVI strength shows a high dependency on these parameters. BVI level rise significantly when the vortex passes though the airfoil closely. The incidence angle of the airfoil also has a noticeable influence on the BVI peak levels.

4. As the incident angle is increased, the peak position of the BVI level shifts to the negative side. The reason of position shift is the existence of upwash ahead of an airfoil with incidence angle. The vortex moves upward while convected downstream in such a flowfield.

The influences of the vortex core size and circulation strength are not studied in this research and remain as future research items.

References

[1] C. Kitaplioglu, F.X. Caradonna, and C.L. Burley, “Parallel Blade-Vortex Interactions: An Experimental Study and Comparison with Computations,” Journal of the American Helicopter Society, pp.272-281, July (1997).

[2] C. Kitaplioglu, F.X. Caradonna, and M. McClur, “An Experimental Study of Parallel Blade-Vortex Interaction Aerodynamics and Acoustics Utilizing and Independently Generated Vortex,” NASA/TM-1999-208790, July (1999).

[3] Y. Tanabe, S. Saito, C. Yang, and T. Aoyama, C. Benoit, J.-O. Gretay, G. Jeanfaivre, S. Peron, J. Sides, “Inviscid Numerical Simulations of 2D Parallel Blade-Vortex Interaction,” JAXA-RR-06-042E, also ONERA Technical Report, No. RT 1/11474 DSNA, March 2007.

[4] S. Lee and D. Bershader, “Head-On Parallel Blade-Vortex Interaction,” AIAA Paper No,91-3277, 9th Appliel Aerodynamics Conference, Baltimore, MD, Sept. 23-26, (1991).

[5] D. Lee, C. Cho, Y. Yu, “Simulation of BVI noise generation using Computational Aeroacoustics,” INTER-NOISE 2006, Honolulu, Hawaii, USA, 3-6 December, (2006).

[6] F. Falissard, A. Lerat, and J. Sidès, “Vortictiy Preserving Sheme for Unsteady Compressible Folw,” 4th International Conference on CFD (ICCFD) GHENT, BELGIQUE 10-14 July (2006)

[7] G.R. Srinivasan, W.J. McCroskey, and J.D. Baeder, “Aerodynamics of Two-Dimensional Blade-Vortex Interaction,” AIAA Journal, Vol. 24, No. 10, pp. 1569-1576, (1986)

[8] A. Ochi, T. Aoyama, S. Saito, E. Shima and E. Yamakawa, “BVI Noise Predictions by Moving Overlapped Grid Method,” 55th American Helicopter Society Annual Forum, May (1999).

[9] M J.Bhagwat, “Generalized Viscous Vortex Model for Application to Free-Vortex Wake and Aeroacoustic Calculations,” 58th Annual Forum and Technology Display of the American Helicopter Society International, Montèal, Canada, June 11-13, (2002).

[10] E. Shima and T. Jounouchi, “Role of CFD in Aeronautical Engineering (No.14) – AUSM Type Upwind Schemes -”, NAL SP-34, 7-12, (1999).

[11] Jameson and T.J. Baker, “Solution of Euler Equations for Complex Configuration,” AIAA Paper 83-1929 (1983).

[12] H.C. Yee, and A. Harten, “Implicit TVD Schemes for Hyperbolic Conservation Laws in Curvilinear Coordinates,” AIAA Journal, 25(2), 266-274, (1987).

JAXA Research and Development Report JAXA-RR-07-051E

Date of Issue : February 29, 2008

Edited and Published by : Japan Aerospace Exploration Agency

7-44-1 Jindaiji-higashimach, Chofu-shi,Tokyo 182-8522,Japan

URL:http://www.jaxa.jp/

Printed by : NORTH ISLAND Co.,Ltd